SAND2018-0640R

Sandia National Laboratories
Operated for the U.S. Department of Energy by
National Technology and Engineering Solutions of Sandia, LLC.
Albuquerque, New Mexico 87185

date: January 22, 2018

to: Troy Skousen, Org. 1557, MS-0840
Julie Harvie, Org. 1557, MS-0840

from: Dan Rohe, Org. 1522, MS-0557

subject: BARC (uncut) Modal Testing with 3D Scanning Laser Doppler Vibrometry

1 Executive Summary

Modal testing was performed on the uncut BARC structure as a whole and broken into its two sub-assemblies. The structure was placed on soft foam during the test. Excitation was provided with a small modal hammer attached to an actuator. Responses were measured using a 3D Scanning Laser Doppler Vibrometer. Data, shapes, and geometry from this test can be downloaded in Universal File Format from the Sandia Connect SharePoint site.

2 Introduction

The Box Assembly with Removable Component (BARC) has been introduced as a challenge problem for boundary conditions in environmental testing (see Appendix A for challenge problem announcement). The BARC consists of two substructures, the base substructure is a box beam and the removable component is made from two C-channels and a beam. 6061 aluminum was used for the component beam and box beam. 6063 aluminum was used for the C-channels. Two versions of the BARC have been manufactured, one with a cut in the box beam between the legs of the component and one without that cut. This memo addresses the uncut BARC structure. Also, note that some boundary condition challenge participants have used adhesives in the joints to reduce nonlinear effects; no such modifications were performed on the structure in this test.

In order to address the questions raised by the boundary condition study, a preliminary experimental modal analysis was desired to both inform analytical models of the structure

Sandia National Laboratories is a multimission laboratory managed and operated by National Technology and Engineering Solutions of Sandia LLC, a wholly owned subsidiary of Honeywell International Inc. for the U.S. Department of Energy's National Nuclear Security Administration under contract DE-NA0003525.

and to use for substructuring calculations. The objective of this modal testing was to provide natural frequencies, damping ratios, and mode shapes.

3 Test Setup

Preliminary testing of the BARC with accelerometers resulted in suspect data, suggesting significant nonlinearities even for the bare box beam substructure, which should intuitively be a linear structure. It was thought that the accelerometer cables were interacting with the lightly damped structure; however because funding at the time was limited, this was not further investigated. Instead when funding became available to do the testing again, a Scanning Laser Doppler Vibrometer system was used to limit the effects of the instrumentation on the response of the part. Figure 1 shows the laser vibrometer system, and Figure 2 shows the test articles in test configuration. To improve laser signal return, retro-reflective tape was applied to all surfaces of the BARC that were measured.

The test articles were placed on soft foam to approximate a free boundary condition. Initially, soft bungee cords were used; however, with that setup the rigid body motions of the part would ring down over a long period of time relative to the elastic motion. In order to handle this long rigid body ring down, several options were available, but none were optimal. If the measurement frame were extended to encompass the entire rigid body ring-down, the elastic motion of the measurement would only represent a small portion of the measurement frame and thus the signal-to-noise ratio would suffer and the frequency response functions would become noisy. Additionally, this would make the measurement take many times longer to make. If the measurement frame were reduced to only encompass the ring-down of the elastic motion, leakage would occur in the measurement as the measured response would not end at zero due to the lingering rigid body motion. A windowing function could have been applied, but in that case leakage would still occur if the part had not been allowed to decay to zero rigid body motion before the next impact, and therefore the measurement would still have taken many times longer to make.

Foam, on the other hand, adds significant rigid body damping to the part which allows the measurements to be made more quickly and reduces effects of leakage. The foam may add a small amount of stiffness and more significant damping to elastic modes, especially the lower frequency modes, so the parts were oriented to minimize these effects.

A small modal hammer (PCB 086E80) with a small extender mass was used to excite the structure. The hammer was automatically actuated using a Maul-Theet automatic hammer system. Impacts were generally kept between 5 and 10 N.

3.1 Acquisition Settings

The data acquisition system of the SLDV was set up to measure vibration spectra (FFT acquisition mode). The bandwidth of system was set to 10,000 Hz due to the high frequency content of the hammer impact. 32,000 samples were measured with a sampling frequency of 25,000 Hz, resulting in 12,800 frequency lines and a frequency resolution of 0.7812 Hz. Each

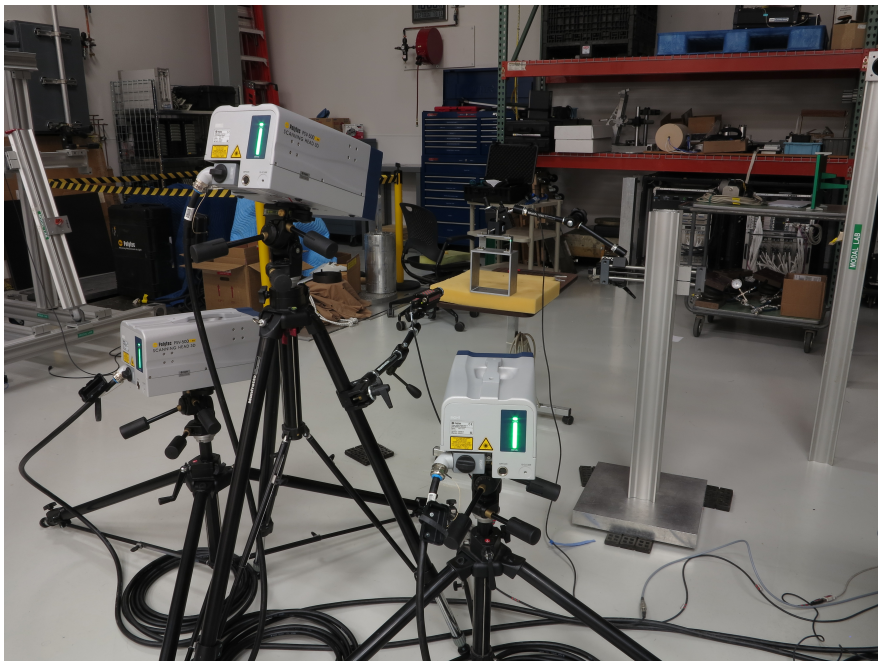

Figure 1: Laser vibrometer system

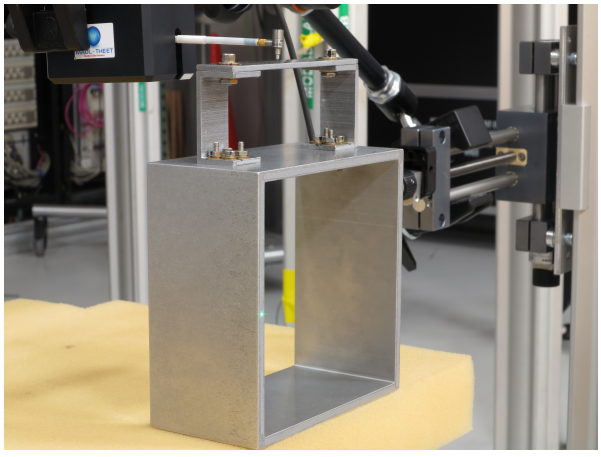

(a) Test setup for testing the BARC as well as for testing only the box beam substructure.

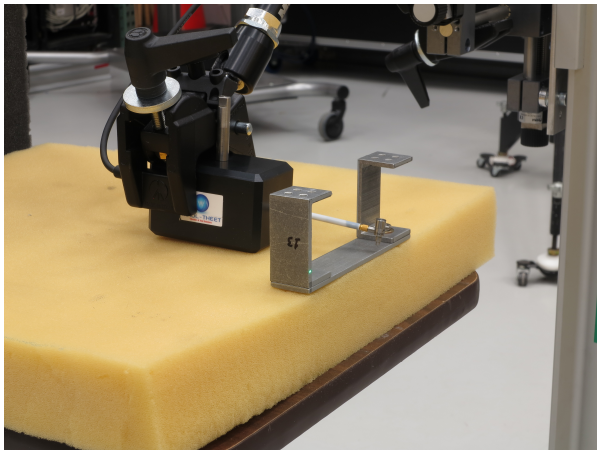

(b) Test setup for testing the removable component.

Figure 2: Test setups showing the boundary conditions, excitation, and laser vibrometer spots.

Table 1: Channel Table for All Scans

Channel	Reference	Point	Dir	Coupling	Quantity	Sensitivity	Range	SE Active
Vibrometer 3D	–	–	3D	DC	Velocity	125.0 mm/s / V	10.0 V	Yes
Channel 1	Ref	Various	Various	AC ICP	Force	60.24 N / V	1.0 V	Yes

measurement took 1.28 seconds. The impact hammer (Channel 1) was used to trigger this test. The trigger was defined as a rising signal with a level of 1%. A pre-trigger value of 1% was used. Complex averaging was used, and 10 averages were specified. No windows or filters were applied to the data. Channel information is shown in Table 1. Signal Enhancement was enabled for channels specified in Table 1. Speckle tracking was enabled and the signal enhancement level was set to Standard. The system was set to automatically remeasure suboptimal data.

3.2 Test Geometry

A test geometry was created to ensure the same points were measured on the individual subcomponent-level tests as were measured on the full assembly test. Points were placed on the $z+$ and $z-$ faces of BARC so that the entire structure could be measured with two scans. The measurement points are numbered so that the 100 series of points is on the $z-$ face of the box, the 200 series is on the $z+$ side of the box, the 300 series is on the $z-$ side of the component, and the 400 series is on the $z+$ side of the component. The test geometry and test coordinate system are shown in Figure 3. The origin of the coordinate system was defined as the corner of the test article such that the entire BARC structure was in the $(+x, +y, +z)$ octant. Measurement point coordinates are enumerated in Tables 2 and 3. Note that in the full assembly test, the points on the component C-channels that are near the mating surface of the box beam could not be measured due to the angle that the laser heads were making with the test article.

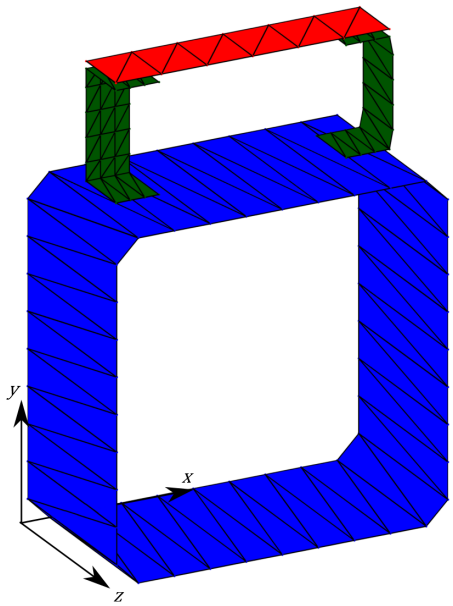

Figure 3: Test Geometry (active content, see Appendix B).

Table 2: Measurement point coordinates on the box beam subassembly

Index	x (cm)	y (cm)	z (cm)
101	1.27	0.32	0.00
102	2.86	0.32	0.00
103	4.44	0.32	0.00
104	6.03	0.32	0.00
105	7.62	0.32	0.00
106	9.21	0.32	0.00
107	10.80	0.32	0.00
108	12.38	0.32	0.00
109	13.97	0.32	0.00
111	14.92	1.27	0.00
112	14.92	2.86	0.00
113	14.92	4.44	0.00
114	14.92	6.03	0.00
115	14.92	7.62	0.00
116	14.92	9.21	0.00
117	14.92	10.80	0.00
118	14.92	12.38	0.00
119	14.92	13.97	0.00
121	13.97	14.92	0.00
122	12.38	14.92	0.00
123	10.80	14.92	0.00
124	9.21	14.92	0.00
125	7.62	14.92	0.00
126	6.03	14.92	0.00
127	4.44	14.92	0.00
128	2.86	14.92	0.00
129	1.27	14.92	0.00
131	0.32	13.97	0.00
132	0.32	12.38	0.00
133	0.32	10.80	0.00
134	0.32	9.21	0.00
135	0.32	7.62	0.00
136	0.32	6.03	0.00
137	0.32	4.44	0.00
138	0.32	2.86	0.00
139	0.32	1.27	0.00
201	1.27	0.32	7.62
202	2.86	0.32	7.62
203	4.44	0.32	7.62
204	6.03	0.32	7.62
205	7.62	0.32	7.62
206	9.21	0.32	7.62
207	10.80	0.32	7.62
208	12.38	0.32	7.62
209	13.97	0.32	7.62
211	14.92	1.27	7.62
212	14.92	2.86	7.62
213	14.92	4.44	7.62
214	14.92	6.03	7.62
215	14.92	7.62	7.62
216	14.92	9.21	7.62
217	14.92	10.80	7.62
218	14.92	12.38	7.62
219	14.92	13.97	7.62
221	13.97	14.92	7.62
222	12.38	14.92	7.62
223	10.80	14.92	7.62
224	9.21	14.92	7.62
225	7.62	14.92	7.62
226	6.03	14.92	7.62
227	4.44	14.92	7.62
228	2.86	14.92	7.62
229	1.27	14.92	7.62
231	0.32	13.97	7.62
232	0.32	12.38	7.62
233	0.32	10.80	7.62
234	0.32	9.21	7.62
235	0.32	7.62	7.62
236	0.32	6.03	7.62
237	0.32	4.44	7.62
238	0.32	2.86	7.62
239	0.32	1.27	7.62

Table 3: Measurement point coordinates on the removable component subassembly

Index	x (cm)	y (cm)	z (cm)
301	1.59	20.48	2.54
302	3.60	20.48	2.54
303	5.61	20.48	2.54
304	7.62	20.48	2.54
305	9.63	20.48	2.54
306	11.64	20.48	2.54
307	13.65	20.48	2.54
311	1.59	15.40	2.54
312	2.22	15.40	2.54
313	2.86	15.40	2.54
314	3.49	15.40	2.54
321	1.59	20.16	2.54
322	2.22	20.16	2.54
323	2.86	20.16	2.54
324	3.49	20.16	2.54
331	1.59	16.19	2.54
332	2.22	16.19	2.54
333	2.86	16.19	2.54
334	3.49	16.19	2.54
341	1.59	17.25	2.54
342	2.22	17.25	2.54
343	2.86	17.25	2.54
344	3.49	17.25	2.54
351	1.59	18.31	2.54
352	2.22	18.31	2.54
353	2.86	18.31	2.54
354	3.49	18.31	2.54
361	1.59	19.37	2.54
362	2.22	19.37	2.54
363	2.86	19.37	2.54
364	3.49	19.37	2.54
371	11.75	15.40	2.54
372	12.38	15.40	2.54
373	13.02	15.40	2.54
374	13.65	15.40	2.54
381	11.75	20.16	2.54
382	12.38	20.16	2.54
383	13.02	20.16	2.54
384	13.65	20.16	2.54
391	13.81	16.19	2.54
392	13.81	17.25	2.54
393	13.81	18.31	2.54
394	13.81	19.37	2.54
401	1.59	20.48	5.08
402	3.60	20.48	5.08
403	5.61	20.48	5.08
404	7.62	20.48	5.08
405	9.63	20.48	5.08
406	11.64	20.48	5.08
407	13.65	20.48	5.08
411	1.59	15.40	5.08
412	2.22	15.40	5.08
413	2.86	15.40	5.08
414	3.49	15.40	5.08
421	1.59	20.16	5.08
422	2.22	20.16	5.08
423	2.86	20.16	5.08
424	3.49	20.16	5.08
471	11.75	15.40	5.08
472	12.38	15.40	5.08
473	13.02	15.40	5.08
474	13.65	15.40	5.08
481	11.75	20.16	5.08
482	12.38	20.16	5.08
483	13.02	20.16	5.08
484	13.65	20.16	5.08
491	13.81	16.19	5.08
492	13.81	17.25	5.08
493	13.81	18.31	5.08
494	13.81	19.37	5.08

3.3 Laser Vibrometer Setup

The 3D Scanning Laser Doppler Vibrometer used in this test was the Polytec PSV-500 Xtra. The lasers were initially aligned to an arbitrary coordinate system using the following approach. 6 non-coplanar 3D alignment points were placed on a reference object. Three of these points were specified as an origin, a point on the x axis, and a point on the x-y plane, and the other three were specified as additional alignment points. The geometry scan unit in the top laser head was used to determine distances from these 6 points to the top laser head. Retro-reflective tape was used on the reference object to improve signal return of the geometry laser. The laser head positions in the arbitrary coordinate system were computed from this alignment. The alignment error was 0.00, 0.48, and 0.40 millimeters for the Top, Left, and Right laser heads, respectively. This coordinate system had no reference to the BARC component, so before any scans could be stitched together, the laser head positions and orientations needed to be transformed from the arbitrary coordinate system into the part coordinate system.

To align the lasers to the part coordinate systems, a transformation was applied to the laser head position and orientation. To solve for this transformation, alignment points were placed on the part at the corners for each individual substructure test. For the full assembly test, six alignment points were used at the four corners of the box beam and at the two corners of the bench. At each of these points, the (x, y, z) coordinate was known in the part coordinate system from the drawings. The (x, y, z) coordinate in the initial arbitrary coordinate system was found by triangulating the laser beams at each point. Given the known positions of the laser heads in the arbitrary coordinate system as well as the laser head mirror deflections, the vector for each laser beam could be computed, and their point of closest intersection was then identified as the alignment point coordinate in the arbitrary coordinate system. Given the coordinates of four or six points in both the arbitrary coordinate system and the part coordinate system, the transformation between the two can be found. Once that transformation was applied to the laser scan head positions and orientations, the laser system was able to accurately position its lasers at measurement points in the part coordinate systems.

For all scans, the measurement point geometry was imported from the test geometry from Section 3.2. Points on the opposite side of the test article or on components not in the current test were deleted. Upon importing the measurement points, the laser system positioned the lasers at each measurement point and identified those points on the camera image. These images are shown in Figure 4.

4 Modal Testing and Analysis

Modal testing was performed by exciting the structure with the automated impact hammer while the laser system scanned the measurement points. Two impact locations were used: an impact location on the box was placed at the measurement point closest to the point denoted in the challenge problem description (see Appendix A), and an impact location near the center of the component's beam excited modes that the box excitation location did not.

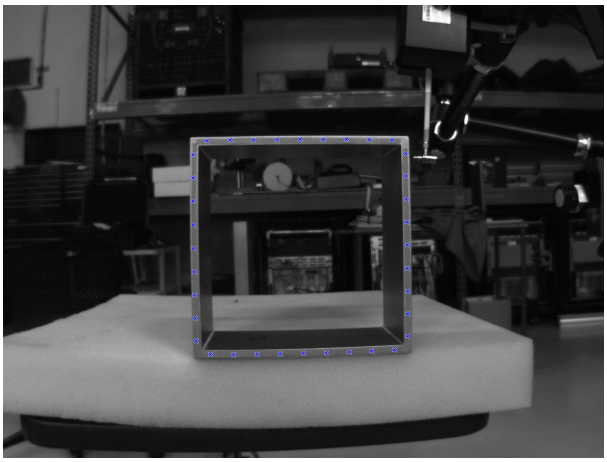

(a) Box $z+$ scan

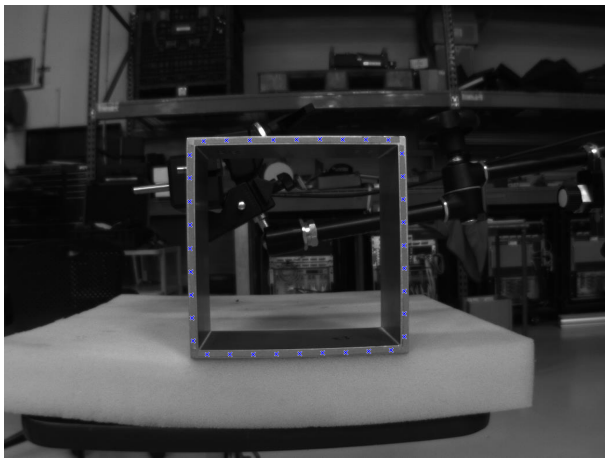

(b) Box z- scan

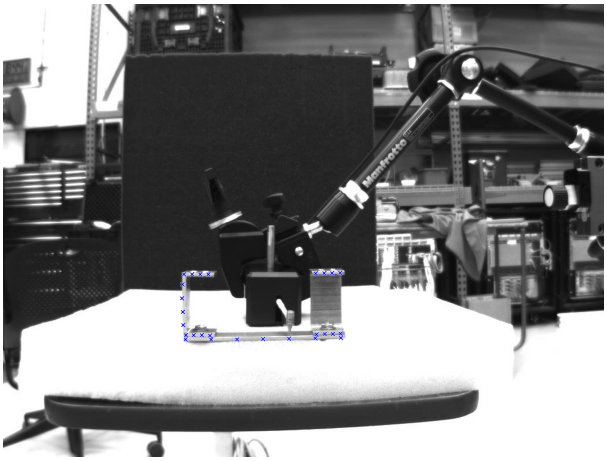

(c) Component $z+$ scan

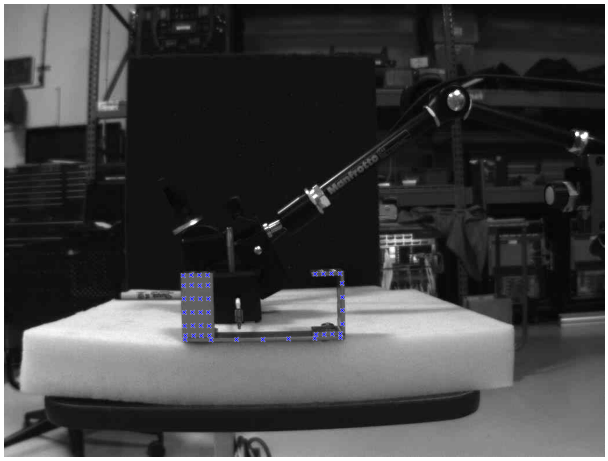

(d) Component z- scan

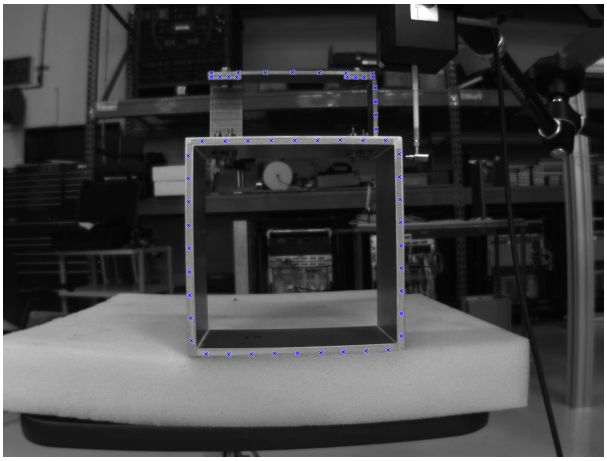

(e) BARC $z+$ scan

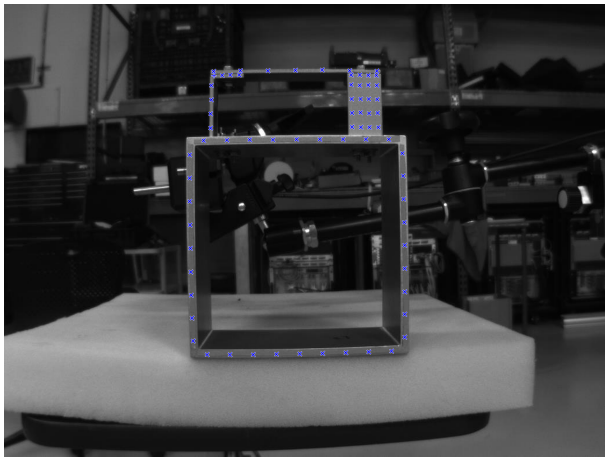

(f) BARC z- scan

Figure 4: Measurement points for the various scans.

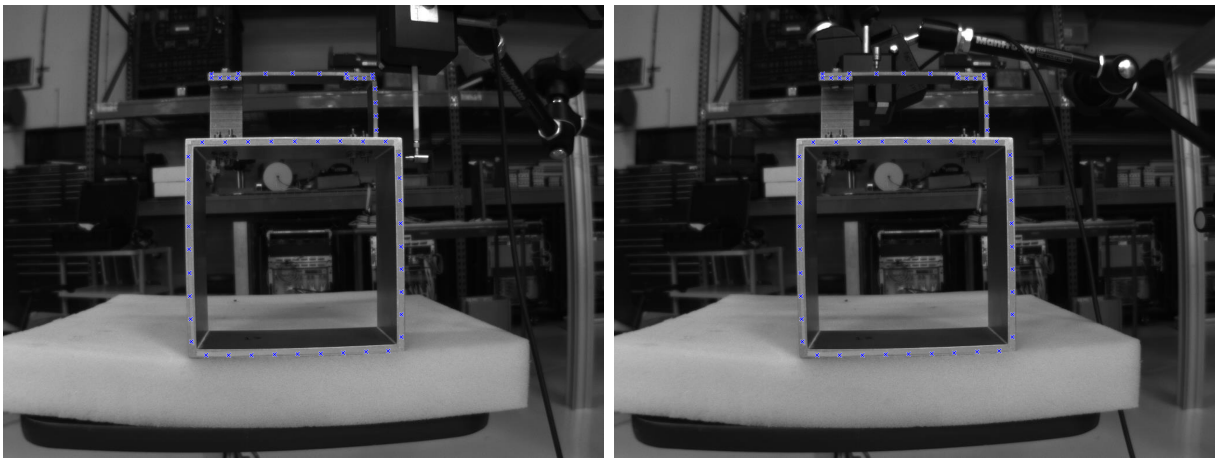

(a) Impact location on the box **(b)** Impact location on the component

Figure 5: Impact Locations on the box and component.

These impact locations are shown in Figure 5. The force to velocity frequency response functions (FRFs) measured by the laser system were differentiated in the frequency domain to produce force to acceleration FRFs that could be used by traditional modal analysis tools. The Synthesize Modes and Correlate (SMAC) algorithm [1] was used to fit modes to the data.

Data from each impact location was fit separately due to nonlinearities in the data that could cause modes to shift from impact location to impact location. The following subsections describe the results of the modal analysis for each component.

4.1 Box Modal Analysis

Modes extracted from the box beam structure are enumerated in Table 4. 34 modes were fit to the box structure between 0 and 10 kHz. Figure 6 shows an experimental complex mode indicator function (CMIF) compared to an analytical CMIF created from FRFs resynthesized from the extracted modes. The modal assurance criterion (MAC) matrix is shown in Figure 7. Mode shapes are shown in Figure 8. Overall good fits to the data were achieved. One mode near 1566 Hz was not able to be extracted from the data. Also, there exist many repeated modes due to the symmetry of the structure. For such modes, due to only one excitation location being impacted for this test, only one of the pair of modes was extracted and reported here. The MAC matrix shows high off-diagonal components for several high frequency modes. These modes are expected to have bulging motion of the faces of the box beam, and because no measurement points were placed on those faces of the box, they look very similar to other modes extracted from the test.

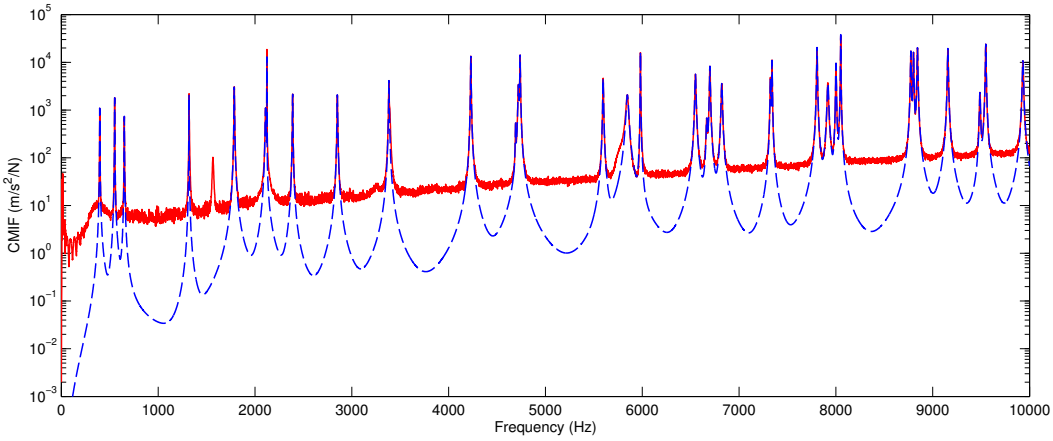

Figure 6: Modal fits for the Box substructure

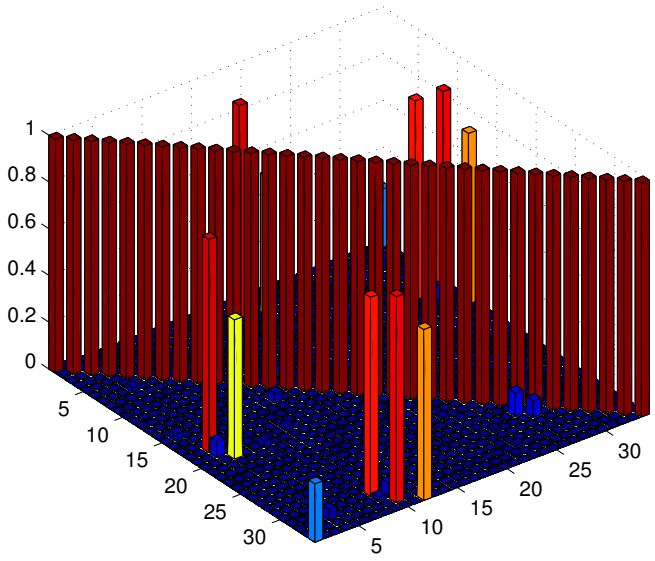

Figure 7: MAC matrix for the Box substructure

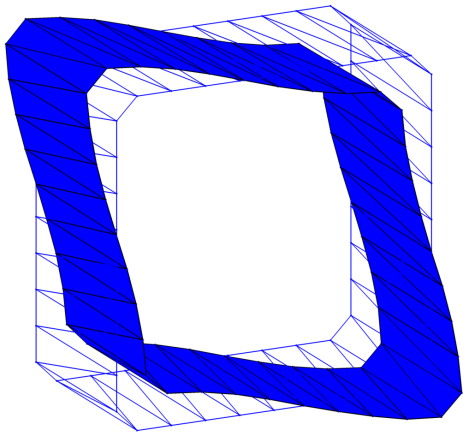

Figure 8: Box Mode Shapes (active content, see Appendix B).

Table 4: Modes extracted from the box beam structure.

Mode	Frequency (Hz)	Damping Ratio
1	397.2	0.263%
2	550.8	0.173%
3	650.9	0.173%
4	1318.5	0.056%
5	1786.3	0.130%
6	2109.1	0.177%
7	2122.3	0.012%
8	2389.1	0.085%
9	2850.8	0.099%
10	3383.6	0.084%
11	4229.7	0.056%
12	4691.8	0.073%
13	4721.3	0.107%
14	4738.2	0.059%
15	5596.1	0.062%
16	5846.1	0.205%
17	5981.3	0.024%
18	6549.2	0.081%
19	6665.7	0.091%
20	6698.5	0.061%
21	6821.1	0.085%
22	7323.7	0.050%
23	7340.2	0.034%
24	7804.7	0.041%
25	7917.2	0.096%
26	8000.8	0.039%
27	8049.2	0.021%
28	8774.2	0.043%
29	8801.6	0.040%
30	8842.2	0.042%
31	9156.3	0.042%
32	9487.5	0.057%
33	9547.7	0.036%
34	9931.3	0.054%

4.2 Component Modal Analysis

Modes extracted from the component structure are enumerated in Table 5. 18 modes were fit to the component structure between 0 and 10 kHz. Figure 9 shows an experimental CMIF compared to an analytical CMIF created from FRFs resynthesized from the extracted modes. The MAC matrix is shown in Figure 10. Mode shapes are shown in Figure 11. Nonlinear effects were seen in the CMIF in Figure 9, likely due to the joint in the component, even at relatively low impact levels of 5-10 N. The low off-diagonal components of the MAC matrix suggests that the measurement points on this structure were able to distinguish all of the modes.

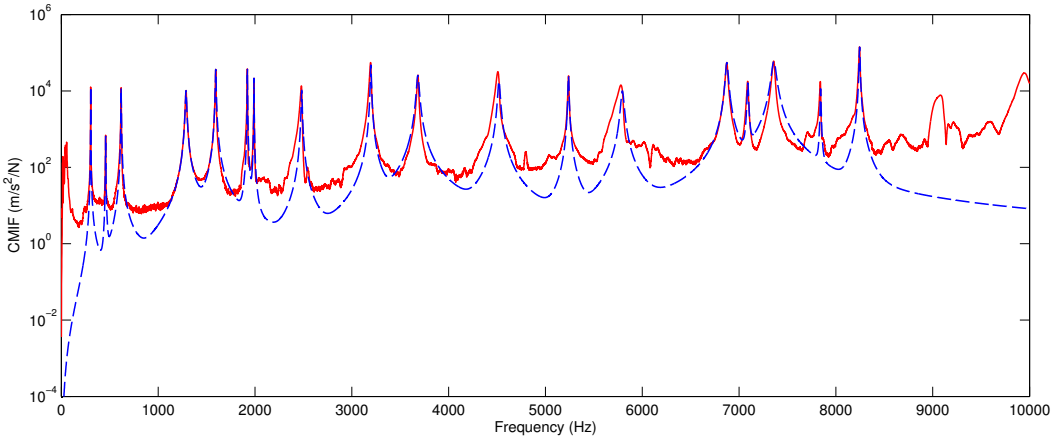

Figure 9: Modal fits for the component substructure

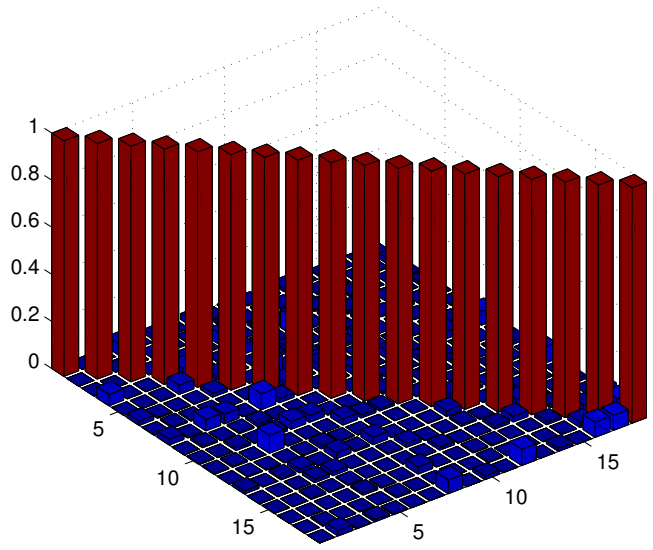

Figure 10: MAC matrix for the component substructure

Table 5: Modes extracted from the component structure.

Mode	Frequency (Hz)	Damping Ratio
1	303.6	0.125%
2	457.8	0.270%
3	618.1	0.258%
4	1287.8	0.493%
5	1594.5	0.235%
6	1921.8	0.064%
7	1989.8	0.059%
8	2482.5	0.195%
9	3196.9	0.152%
10	3682.2	0.353%
11	4520.1	0.253%
12	5238.0	0.092%
13	5794.5	0.267%
14	6873.6	0.194%
15	7090.3	0.093%
16	7358.9	0.313%
17	7841.8	0.049%
18	8244.7	0.054%

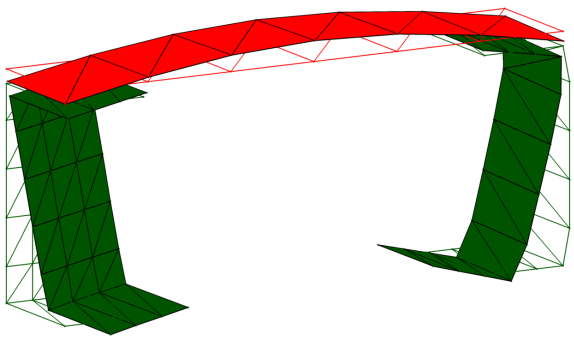

Figure 11: Component Mode Shapes (active content, see Appendix B).

4.3 BARC Modal Analysis

Modes extracted from the BARC are enumerated in Tables 6 and 7. 52 modes were fit to the BARC between 0 and 10 kHz from the impact location on the box, and 46 modes were fit from the impact location on the component. Figure 12 shows experimental CMIFs compared to an analytical CMIFs created from FRFs resynthesized from the extracted modes. The MAC matrix is shown in Figure 10. Mode shapes are shown in Figures 14 and 15. Nonlinear effects were seen in the CMIF in Figure 12a, similar to in the component test, even at relatively low impact levels of 5-10 N. The data from the box impact showed significantly less nonlinearity.

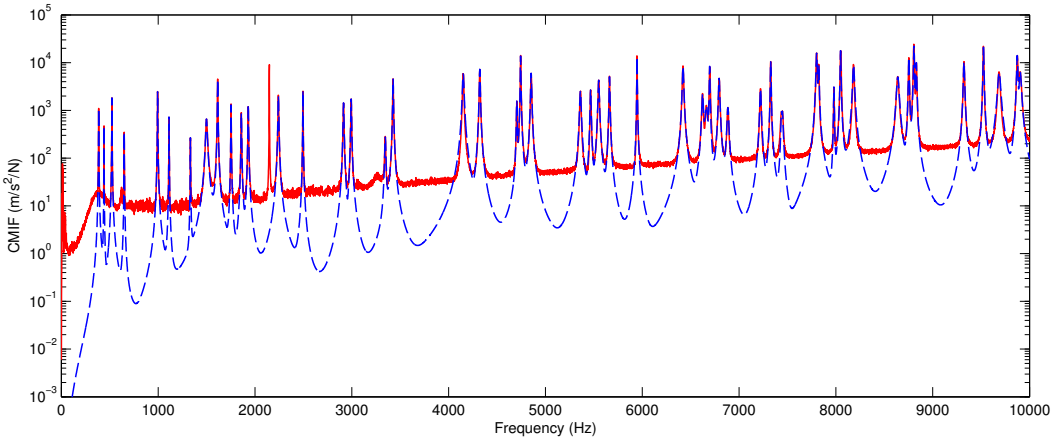

(a) Impact location on the box

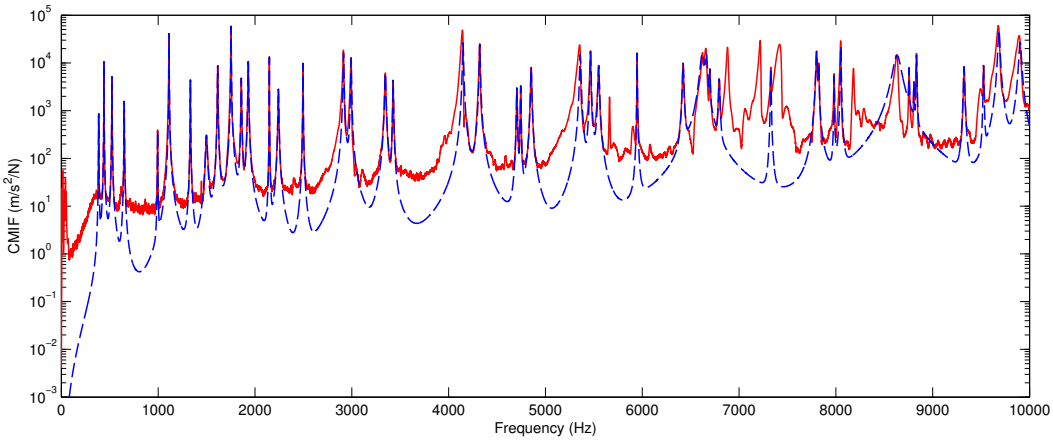

(b) Impact location on the component

Figure 12: Modal fits for the BARC

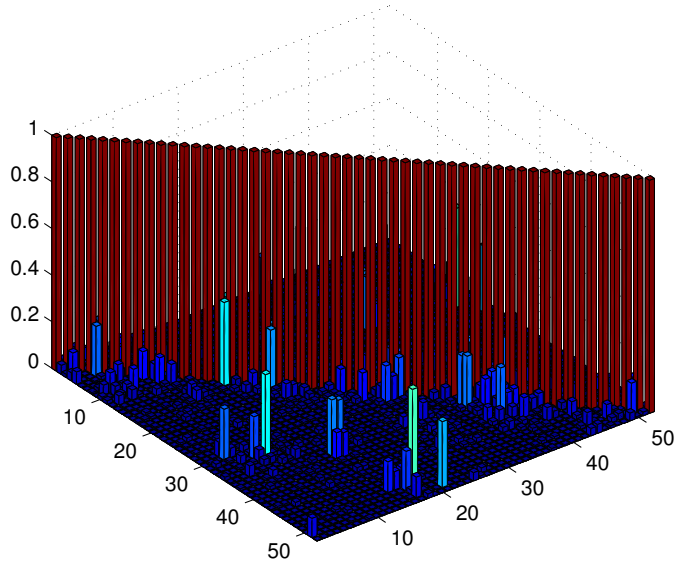

(a) Impact location on the box

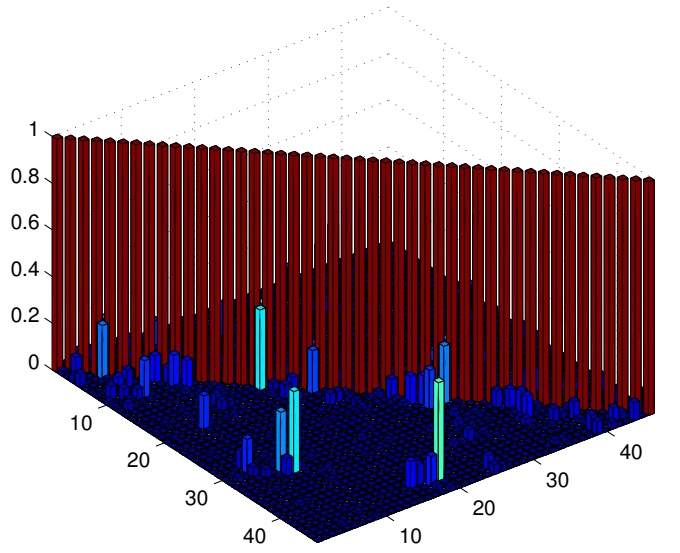

(b) Impact location on the component

Figure 13: MAC matrices for the BARC component

Table 6: Modes extracted from the BARC structure from an impact on the box.

Mode	Frequency (Hz)	Damping Ratio
1	385.6	0.263%
2	440.7	0.146%
3	522.8	0.202%
4	649.8	0.170%
5	994.3	0.146%
6	1112.8	0.107%
7	1333.3	0.104%
8	1499.2	0.569%
9	1614.9	0.140%
10	1752.7	0.097%
11	1859.4	0.143%
12	1930.5	0.147%
13	2242.0	0.165%
14	2495.3	0.062%
15	2914.8	0.143%
16	2993.8	0.124%
17	3346.1	0.168%
18	3426.6	0.101%
19	4150.8	0.193%
20	4321.9	0.108%
21	4703.9	0.085%
22	4743.3	0.061%
23	4852.3	0.107%
24	5360.9	0.144%
25	5466.4	0.092%
26	5550.0	0.114%
27	5661.7	0.071%
28	5946.1	0.035%
29	6421.1	0.104%
30	6623.0	0.116%
31	6662.5	0.213%
32	6695.9	0.053%
33	6793.8	0.098%
34	6884.4	0.134%
35	7221.1	0.099%
36	7326.6	0.049%
37	7436.9	0.070%
38	7447.2	0.104%
39	7800.7	0.077%
40	7822.6	0.058%
41	7979.7	0.041%
42	8047.9	0.046%
43	8182.0	0.108%
44	8639.1	0.152%
45	8753.1	0.047%
46	8806.1	0.048%
47	8830.6	0.053%
48	9322.7	0.064%
49	9524.2	0.044%
50	9685.9	0.154%
51	9872.7	0.060%
52	9903.3	0.118%

Table 7: Modes extracted from the BARC structure from an impact on the component.

Mode	Frequency (Hz)	Damping Ratio
1	385.6	0.259%
2	440.6	0.162%
3	522.8	0.208%
4	649.5	0.203%
5	994.5	0.147%
6	1112.6	0.093%
7	1333.1	0.098%
8	1498.1	0.584%
9	1614.8	0.135%
10	1753.2	0.088%
11	1859.1	0.146%
12	1931.0	0.133%
13	2148.7	0.028%
14	2242.2	0.159%
15	2496.1	0.053%
16	2914.7	0.129%
17	2992.9	0.116%
18	3346.1	0.165%
19	3426.6	0.097%
20	4148.4	0.127%
21	4321.4	0.106%
22	4704.7	0.082%
23	4744.5	0.062%
24	4852.3	0.106%
25	5359.4	0.116%
26	5465.6	0.083%
27	5550.0	0.113%
28	5946.9	0.028%
29	6421.9	0.099%
30	6619.5	0.338%
31	6661.8	0.153%
32	6698.3	0.066%
33	6794.5	0.099%
34	7327.6	0.041%
35	7800.0	0.092%
36	7822.3	0.053%
37	7982.0	0.035%
38	8050.4	0.040%
39	8631.3	0.493%
40	8755.5	0.043%
41	8805.5	0.052%
42	8832.7	0.043%
43	9323.4	0.061%
44	9525.0	0.038%
45	9683.7	0.099%
46	9902.7	0.128%

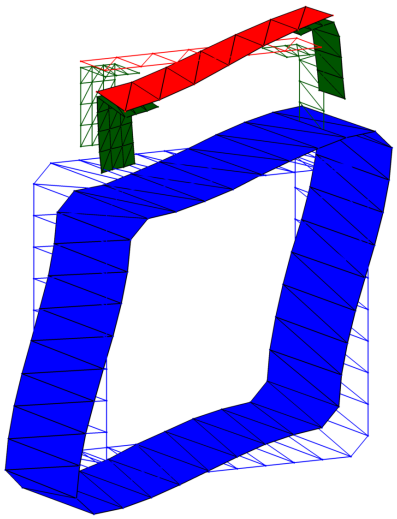

Figure 14: BARC mode shapes extracted from the box impact (active content, see Appendix B).

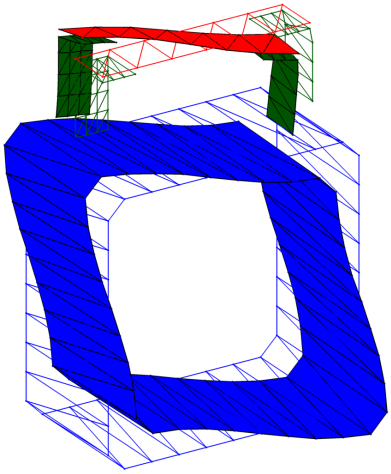

Figure 15: BARC mode shapes extracted from the component impact (active content, see Appendix B).

References

[1] D. P. Hensley and R. L. Mayes, "Extending SMAC to multiple reference FRFs," in *Proceedings of the 24th International Modal Analysis Conference*, (St. Louis, Missouri), pp. 220–230, Jan. 2006.

A BARC Challenge Problem

The next pages are the BARC challenge problem announcement that was sent out to interested parties.

Boundary Conditions in Environmental Testing Challenge Problem

Problem Statement

The current practices for shock & vibration testing of components may result in incorrect damage exposure as compared to that experienced in the full assembly. The difference in boundary conditions has been identified as a major contributor, and may result in components being over- or under-stressed as compared to the intended exposure. A test bed has been developed by the Kansas City National Security Campus in conjunction with Sandia National Laboratories to study and hopefully overcome the boundary condition differences. The physical properties of the test bed are outlined below.

Objective

The objective of this problem is to design a component-level test setup that allows the component to undergo a similar environmental exposure as it experiences in the full assembly. The primary aspects to consider include test specification development and fixture design. Proof of concept may be demonstrated either analytically, experimentally, or a combination of both. The component test must be physically realizable, using fixtures and specifications that are compatible with existing software and test equipment.

Test Bed Description – Box Assembly with Removable Component (BARC)

Part Description

- Component = two C-channels + beam
- Subassembly = box beam
- Assembly = component + subassembly
- Complete part drawings and vendor information are provided in the appendix

Material Properties

- Aluminum (see appendix)

System Boundary conditions

- Free-free

System Assembly

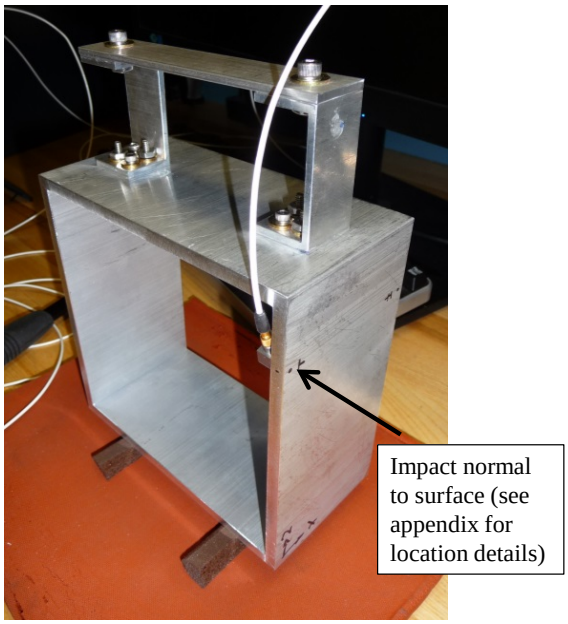

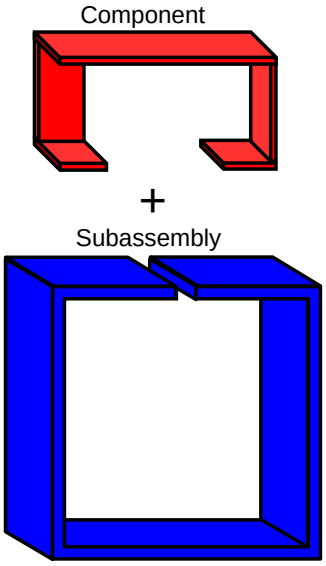

Component Test

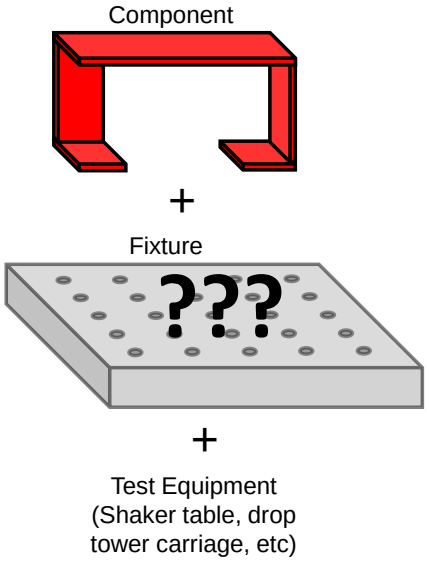

System Environments

- **Suggested Environment – Shock**
  Modal hammer input with nylon tip, approximately 7 lb amplitude with 0.8ms duration[1]. Input location defined in drawing (see appendix).
  - A set of "truth data" in the system environment will be experimentally measured by the organizers and can be provided upon request. Contact Julie Harvie for more information. This is intended to allow the participants to focus their efforts on designing the component test.
- **Additional Environments**
  Other environments may be investigated as desired but will not be the focus of discussion at this time. Future efforts will focus on random vibration environments.

GUIDELINES FOR ASSEMBLING

Component

- Bolt Torque = 50 inch-lb
- Dry connection (no lubrication)

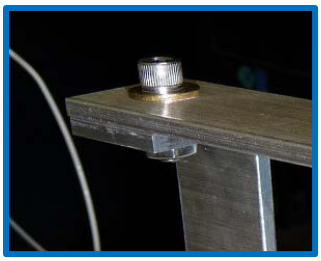

Assembly

- Bolt Torque = 20 inch-lb
- Dry connection (no lubrication)
- Configure bolts in alternating directions as shown

ORGANIZERS

Julie Harvie, Sandia National Laboratories
Tyler Schoenherr, Sandia National Laboratories
Troy Skousen, Sandia National Laboratories
Richard Jones, Kansas City National Security Campus
David Soine, Kansas City National Security Campus

CONTACT INFORMATION

Julie Harvie
Sandia National Laboratories
(505) 284-8292
jharvie@sandia.gov

---

[1] The force input may be approximated analytically using the formula: $F(t) = 7\ \sin^2\left(\frac{\pi}{0.0008}t\right)$
where F is force in pounds and t is time in seconds. Zero-padding should be used to allow adequate response ring-down and frequency resolution.

PART NUMBER	REVISIONS			
	ISS	SHEET ZONE	DESCRIPTION	DATE
PS62955-100			ORIGINAL ISSUE	31-May-17

NOTES

1. ALL DIMENSIONS ARE IN INCHES.
2. BREAK EDGES .030 MAX RADIUS OR CHAMFER.
3. MCMASTER CARR
   200 AURORA INDUSTRIAL PKWY.
   AURORA, OH 442-8087

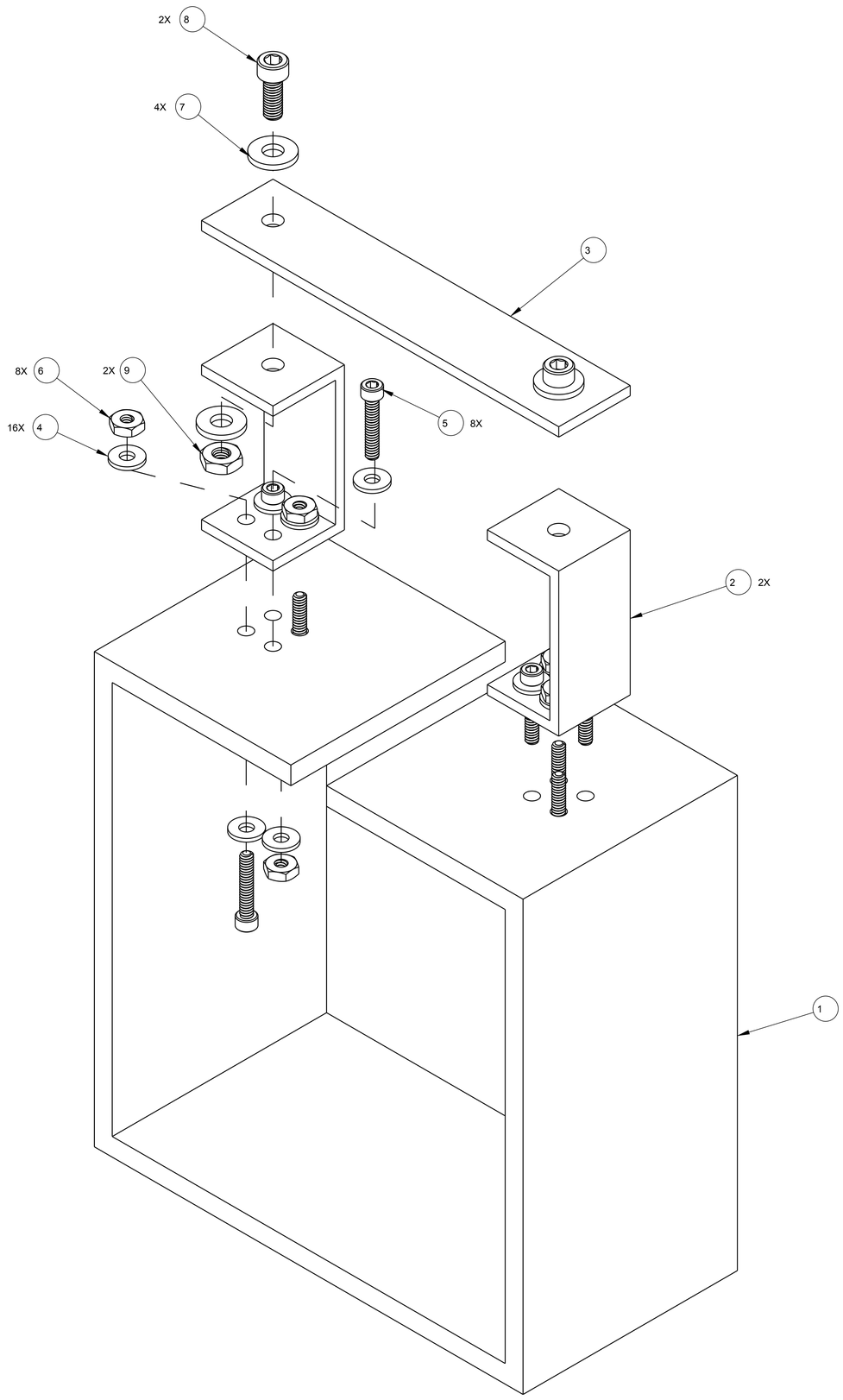

SCALE 2/1

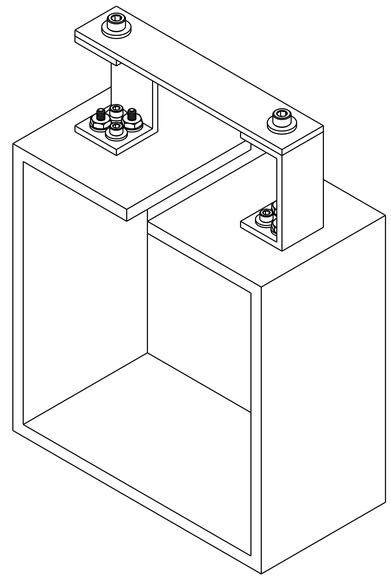

NO REQD	PART/CONTROL NO	DESCRIPTION/MATERIAL	NOTE	SHEET ZONE	ITEM
2	90257A411	316 STAINLESS STEEL SOCKET HEX NUT, 10-32 THREAD SIZE	3		9
2	92185A989	316 STAINLESS STEEL SOCKET HEAD SCREW, 10-32 THREAD SIZE, 1/2" LONG	3		8
4	98023A114	YELLOW ZINC PLATED GRADE 8 STEEL WASHER, 0.22" ID X 0.5" OD	3		7
8	90257A007	316 STAINLESS STEEL HEX NUT, 6-32 THREAD SIZE	3		6
8	92185A151	316 STAINLESS STEEL SOCKET HEAD SCREW, 6-32 THREAD SIZE, 3/4" LONG	3		5
16	98023A112	YELLOW ZINC PLATED GRADE 8 STEEL WASHER, .0156" ID X .0375" OD	3		4
1	8975K578	6061 ALUMINUM, RECTANGULAR BAR, 1/8" X 1", 2' LONG	3	2/A1	3
2	9001K74	6063 ALUMINUM U-CHANNEL, 1/8" WALL THICKNESS, 1" HIGH X 2" WIDE	3	2/C1	2
1	6546K37	6061 ALUMINUM RECTANGULAR TUBE, 1/4" WALL THICKNESS, 6"x6", 3' LENGTH	3	2/A1	1
NA	9919100	MARKING, GENERAL METHODS			
NA	9900000	GENERAL REQUIREMENTS			

CURRENT ISSUE APPROVALS		DATE
DRAWN:	L. WEATHERBY 832KC	-
CHECKED:	MODEL CHECK	
DESIGNED:	RICHARD JONES JR 856KC	
APPROVED:	RICHARD JONES JR 856KC	

QUANTITY NA = NO QUANTITY FOR DOCUMENTS PM = PROCESS MATERIAL AR = AS REQUIRED
ABBREVIATIONS: ALT = ALTERNATE EM = EXPENSE MATERIAL ARS = AS REQUIRED FOR ASSEMBLY

PS62955-100

DRAWING: PS62955-UNC
MODEL: PS62955-100-UNC
TYPE: ASSEM

NSC NATIONAL SECURITY CAMPUS 14520 BOTTS ROAD KANSAS CITY, MO. 64147

ENGLISH

THIRD ANGLE PROJECTION

TITLE: MOCKASSEM2 (U)

PART CLASSIFICATION: UNCLASSIFIED

DRAWING CLASSIFICATION: UNCLASSIFIED

SIZE: E

DRAWING NUMBER: PS62955

ISSUE: -

CAGEC 14061 SCALE 1/1 SHEET 1 OF 2

ORIGIN: CREO-3.0

PDM STATUS: KC - - 31-May-17

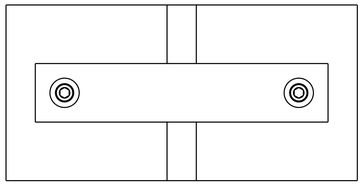

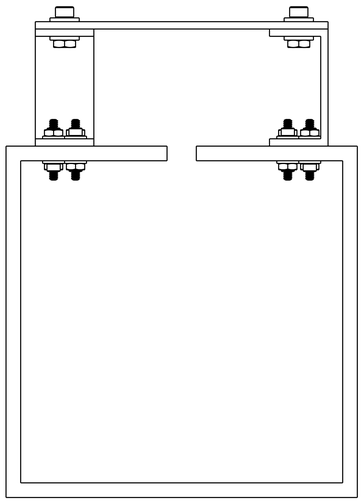

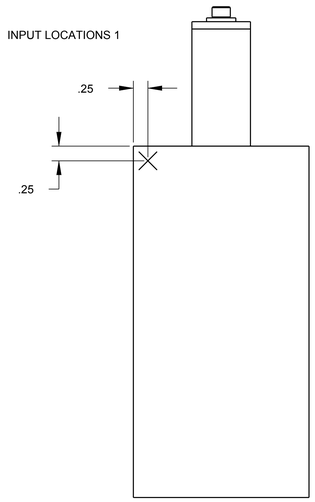

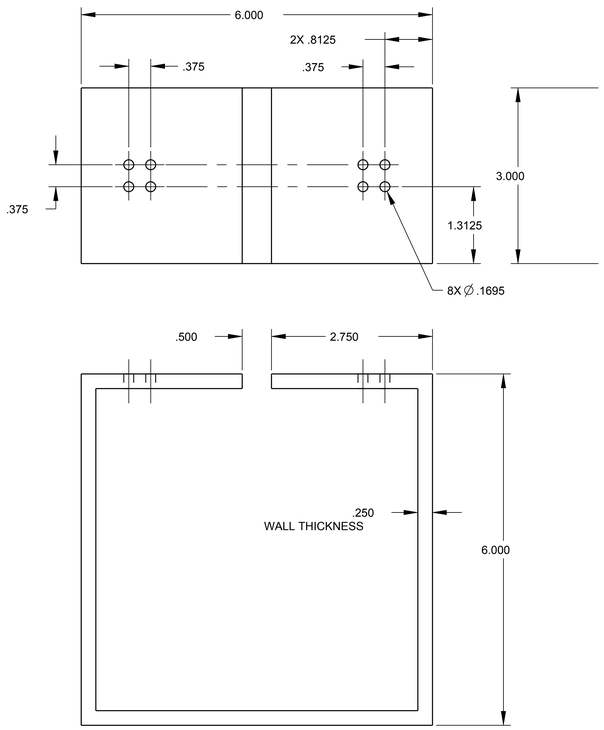

DETAIL ITEM 1
SCALE 1/1

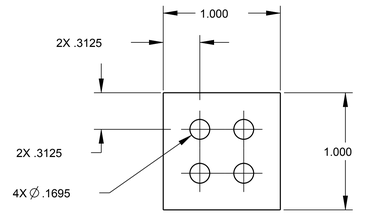

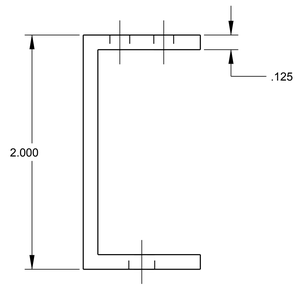

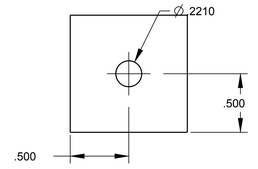

DETAIL ITEM 2
SCALE 2/1

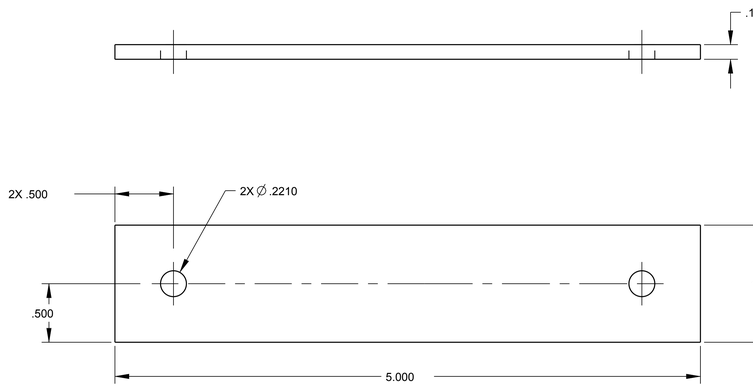

DETAIL ITEM 3
SCALE 2/1

DRAWING NUMBER	PS62955		
DRAWING CLASSIFICATION	UNCLASSIFIED		
SIZE E	CAGEC 14061	SCALE 1/1	
	ISSUE	SHEET 2 OF 2	
PDM STATUS KC -	- 18-Apr-17		

B Active Content

As test models get larger, it can become difficult to convey a potentially complex three dimensional motion on a single two-dimensional image. The two dimensional line drawings typically used to display mode shapes can be even more difficult to interpret because three-dimensional cues such as shadowing, occlusion, and foreshortening are often missing or difficult to see. It can therefore be difficult to develop an intuitive sense of the mode shape and geometry from a two dimensional image.

In this test memo, a 3D model of the test geometry is embedded into this PDF file for some figures, and that 3D model is animated using small JavaScript programs for each mode shape. These 3D animations can be viewed with a sufficiently updated Adobe Reader software with JavaScript enabled. Adobe Reader should query the user to enable JavaScript when such a figure is activated. Alternatively, JavaScript can be enabled in the Preferences menu under the JavaScript category (`Edit` → `Preferences...` → `JavaScript` → `Enable Acrobat JavaScript`), though this method will enable JavaScript for all documents and may present a security risk if untrusted PDFs are downloaded from the Internet, for example. It is better to enable JavaScript for only trusted documents. If the reader does not use Adobe Reader to view PDFs or is uncomfortable with enabling JavaScript for this document, a 2D representation of the figure is still available.

To control the animation, one must first activate the content by clicking on the still image. If the model does not begin its animation, it likely means that JavaScript is not enabled. The animation can be rotated by clicking and dragging on the animation with the left mouse button. The scroll wheel can be used to zoom in and out. If a scroll wheel is not available, the animation can be zoomed by holding the Shift key and while clicking and dragging the animation with the left mouse button or by clicking and dragging with the right mouse button. To pan the animation, simply hold the Control key and click and drag the left mouse button. Additional view options can be accessed by right-clicking on the animation.

The animated shape in each image can be changed to a different mode shape. To change the mode shape that is animated, the reader can right-click on the animation and select 'Next Mode' or 'Previous Mode' from the context menu. Alternatively, the reader can simply press the comma (,) or period (.) keys to view the previous or next mode, respectively. Note that the reader will first need to click within the animation to make it the active animation before the keyboard shortcuts will work. When the mode shape is changed, the JavaScript console will appear and notify the reader which mode is now displayed in that panel.